On the Peak Truncation Approximation of Phase Function for Radia-tive Transfer

Sci. Rep. Tôhoku Univ., Ser. 5, Geophysics, Vol. 24, No. 3, pp. 89–102, 1977.

On the Peak Truncation Approximation of Phase Function for Radiative Transfer

TERUYUKI NAKAJIMA and SHOJI ASANO

Geophysical Institute, Tohoku University, Sendai 980, Japan

(Received June 11, 1977)

Abstract: Accuracy of the peak truncation approximation for radiative transfer of a phase function with a sharp forward scattering peak is investigated for widely differing values of such parameters as incident angle, optical thickness and absorption. Two types of phase functions are considered: one is for water clouds and the other is for hydrosols, where the latter phase function doesn't exhibit a distinct diffraction peak. Errors introduced by the approximation in the emerging fluxes from the cloud layer are smaller than those for the hydrosol layer, because considerable portion of the truncated part of the cloud phase function locates around a smaller scattering angle than that for the hydrosol phase function. Behavior of error profiles for the reflected and transmitted fluxes with respect to the parameters is complicated but systematic. A physical interpretation for the profiles is proposed according to a simple scattering model. Generally errors due to the approximation are small enough and unimportant for most applications. This assures usefulness of the approximation for the multiple scattering problem with a phase function having a sharp forward peak.

1. Introduction

Scattering of light by particles larger than the wavelength of interest is characterized by a signfiicantly anisotropic phase function with a very sharp diffraction peak at the forward direction, of which presence greatly increases the computational difficulty in the multiple scattering problem. It has been shown that the multiple scattering problem with a phase function having a sharp diffraction peak can be greatly simplified by truncating the peak and copensating for this by changing the volume scattering coefficient, and that the error introduced by this approximation may be unimportant for most applications. (Hansen, 1969; Potter, 1970).

Hansen studied the reflection from the conservative atmosphere (single scattering albedo $w_0=1$) and showed that the peak-truncated cloud phase function yields results practically identical to those obtained with the complete cloud phase function, not only for albedos but also for the angular distribution of the reflected intensities. And he showed that the approximation introduces small error in reflectivity of less than 1% for most angles of incidence and emergence, except for direct backscattering, for near-grazing emergent angle and for total scattering angles near 0°, where errors are noticeable, say, several per cent.

Potter (1970) applied the truncated peak approximation to the problem of diffuse transmission and reflection from the conservative ($w_0=1$) and absorptive ($w_0=0.91$) atmospheres. He showed that the accuracy of the approximation for the transmitted and reflected fluxes is within 1% for widely differing values of the incident angle and

optical depth, except for the incident angles $\theta_0 \geqq 84°$.

We have used the truncation approximation in the studies of the transfer of solar radiation in water clouds (Tanaka et al., 1976) and in oceans (Tanaka and Nakajima, 1977). The single scattering albedo w_0 for water clouds becomes very small in the gaseous absorption bands in the near infrared region. It is also the case for oceans where w_0 takes the value ranging from 0.9 to 0.1 in the wavelength region $\lambda=0.45$–0.55 μm. It is important to examine the applicability of truncation approximation to such strong absorbing cases or to cases of very low single scattering albedo. In addition, the phase function for hydrosols doesn't exhibit a distinct diffraction peak, though it is very steep in the forward direction. Errors which would be introduced by truncating the forward scattering peak of the hydrosol-type phase function has not been investigated yet.

In this study we estimate errors introduced by the approximation in the transmitted and reflected fluxes from the scattering layer having the cloud-type phase function and hydrosol-type one for widely varying values of the single scattering albedo and the optical thickness. And we try to physically interpret the behavior of error by considering a simple scattering model.

2. Truncation of phase function

The truncated peak approximation is to consider the photons scattered into the narrow forward peak as not being scattered at all. This removes the peak from the phase function and compensates for the total scattering coefficient. The compensation is to reduce the scattering coefficient by an amount proportional to the fraction truncated from the complete phase function. Then the single scattering albedo w_0 and the optical thickness τ are reduced, respectively, to w_{0t} and τ_t for the truncated phase function as

$$w_{0t} = \frac{(1-S_t)w_0}{1-S_t w_0}\,, \tag{1}$$

$$\tau_t = (1-S_t w_0)\tau\,, \tag{2}$$

where S_t is a truncation ratio defined by Eq. (4).

Two phase functions are adopted; one is for water clouds and the other is for hydrosols. The former has a distinct forward diffraction peak, but the later doesn't exhibit the peak although it is very dominant in the forward scattering.

The cloud phase function used here is shown in Fig. 1 by solid line. It has calculated from Mie theory for the altostratus cloud model at wavelength 1 μm with the complex refractive index $1.326-2.82\cdot10^{-6}\,i$ (Tanaka et al., 1976). The truncated phase function is assumed to be

$$P_t(\cos\Theta) = \begin{cases} a\exp(b\Theta)\,, & \text{for } \Theta \leqq \Theta_t\,, \\ P(\cos\Theta)\,, & \text{for } \Theta \geqq \Theta_t\,, \end{cases} \tag{3}$$

where $P(\cos\Theta)$ and $P_t(\cos\Theta)$ are original and truncated phase functions, respectively,

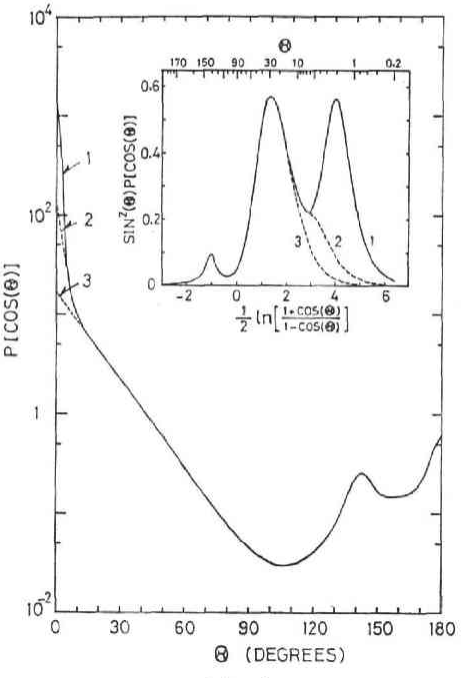

Fig. 1

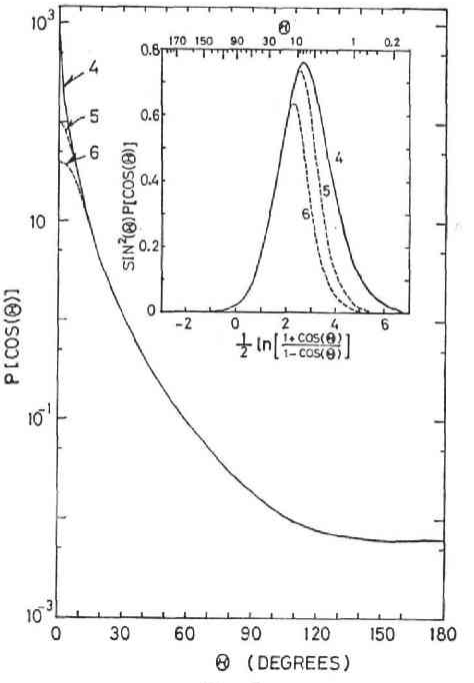

Fig. 2

Fig. 1. Phase functions for scattering by water clouds. Curve 1, untruncated complete phase function; curve 2, peak-truncated phase function with Eq. (3) at the scattering angle $\Theta_t=6°$ with the ratio $S_t=0.3366$; cruve 3, same as cruve 2 but for $\Theta_t=15°$ and $S_t=0.4313$. The transformed picture of $\sin^2\Theta\ P\ (\cos\Theta)$ versus $1/2\ \ln[(1+\cos\Theta)/(1-\cos\Theta)]$ is inserted in the upper part of the figure.

Fig. 2. Same as Fig. 1 but for scattering by hydrosols. Curve 4, untruncated complete phase function; curve 5, peak-truncated phase function with Eq. (5) at $\Theta_t=10°$ with $a=0.014704$, $b=1.007712$, $g=0.0094352$ and $S_t=0.2466$; curve 6, same as curve 5, but for $\Theta_t=15°$, $a=0.018572$, $b=1.007458$, $g=0.020174$ and $S_t=0.4145$.

and Θ is the scattering angle. The constants a and b are determined so as to connect smoothly both profiles at $\Theta=\Theta_t$, by taking the slope of the logarithm of the truncated phase function as being constant for the scattering angles less than Θ_t with the slope equal to that of the untruncated phase function at the scattering angle Θ_t. Then, of course, the truncated phase function must be normalzied properly. In Fig. 1, the cloud phase functions truncated at $\Theta_t=6°$ and $15°$ are shown by broken lines.

In order to see more clearly the scattering ability of the phase function, there is inserted in Fig. 1 the figure of transformed phase function $\sin^2\Theta\cdot P(\cos\Theta)$ as a function of $1/2\ \ln[(1+\cos\Theta)/(1-\cos\Theta)]$. By the definition, the area enclosed by the profile and the scattering angles Θ_1 and Θ_2 gives the scattering ability in the scattering angle between Θ_1 and Θ_2, i.e., $\int_{\cos\Theta_2}^{\cos\Theta_1} P(\cos\Theta)d(\cos\Theta)$. From this figure it can be seen that the cloud phase function has three maxima of the scattering ability such as one caused by diffraction around $\Theta=2°$, one caused by refraction and reflection around $\Theta=30°$, and one corresponding to the rainbow near $\Theta=140°$. The truncation approximation at $\Theta_t=6°$ and $15°$ removes the diffraction peak and the ratios S_t of the

truncated fraction to the total scattering ability amount of 33.66% and 43.13%, respectively, where the truncation ratio S_t is defined by

$$S_t = \int_{4\pi} (P - P_t) d\Omega / 4\pi \,. \tag{4}$$

Since most of the truncated part locates around $\Theta = 2°$, the error introduced by the truncation in the reflected and transmitted fluxes for the cloud layer will be small, although the truncation ratio is large.

Another phase function for hydrosols is shown in Fig. 2 by the solid line. The phase function was computed for the hydrosol model with the complex refractive index 1.07–0.01 i at wavelength 0.5 μm (Tanaka and Nakajima, 1977). The forward peak of the phase function is truncated by the profile;

$$P_t(\cos\Theta) = \begin{cases} \dfrac{a}{(b - \cos\Theta)^2 + g^2} \,, & \text{for } \Theta \leqq \Theta_t \\ P(\cos\Theta) \,, & \text{for } \Theta \geqq \Theta_t \,. \end{cases} \tag{5}$$

The constants a, b and g can be determined to connect smoothly both profiles at $\Theta = \Theta_t$, if $P_t(1)/P_t(\cos\Theta_t)$ is properly given. The truncated phase functions at $\Theta_t = 10°$ and 15° are given in Fig. 2 by broken lines. This truncation procedure seems suitable for the hydrosol phase function because the truncation by Eq. (3) applied to this phase function will turn out to be too steep in the forward scattering angles. The transformed figure of the phase functions inserted in the upper part of Fig. 2 shows that unlike the cloud phase function, the diffraction and refraction peaks are combined in one large peak and, therefore, the truncation procedure does not removes only the diffraction peak. The truncation procedure by Eq. (5) with $\Theta_t = 10°$ and 15° truncates the fraction $S_t = 24.66$ and 41.45% of the total scattering ability, respectively. Although the truncation ratio S_t is smaller than that of the cloud phase function, effects of the truncation would be larger because the considerable portion of the truncated parts locates around the greater scattering angles 5–10°.

Fig. 3 shows the coefficients a_l in the Legendre polynomial expansions of the normalized phase function, that is,

$$P(\cos\Theta) = \sum_{l=0}^{M} a_l P_l(\cos\Theta) \,, \tag{6}$$

where P_l $(\cos\Theta)$ is the Legendre polynomial of order l and M is the maximum order of the expansion. From the figure, we know how the truncation approximation reduces the number of expansion terms of the phase functions and simplifies the angular integration of the radiative transfer equation involving the phase function. For example, an integral of a function involving a phase function over the interval (–1, +1) will be approximated by a finite summation with $(M+1)/2$th order Gaussian quadrature, assuming that other integrands vary slowly (Chandrasekhar, 1960). In Fig. 3, the profile 1 corresponds to the untruncated phase function of the cloud, which needs about 160

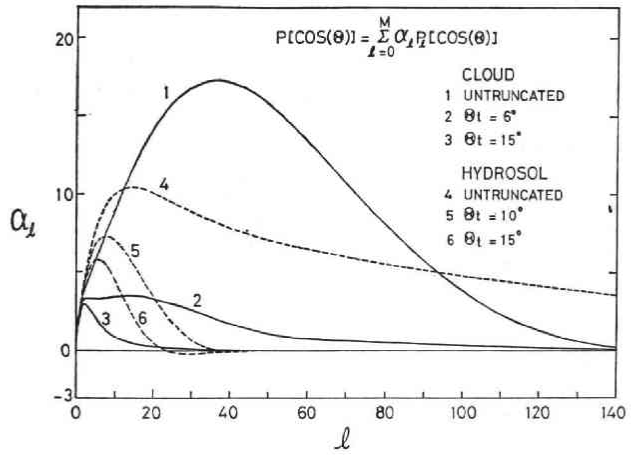

Fig. 3. Coefficients α_l in the Legendre polynomial expansions of the phase functions shown in Figs. 1 and 2.

terms of the expansion, so that more than 80 angular division points are necessary to integrate the phase function with sufficient accuracy. Profiles 2 and 3 correspond to the cloud phase functions truncated by Eq. (3) with $\Theta_t=6°$ and 15°, respectively. Convergence of the profiles is well established at much lower order of the expansion. Especially, for the profile 3 only about 30 angular division points seem to be sufficient for the integration. The profile 4 shows the expansion coefficients of the complete hydrosol phase function. Unlike that of cloud, a flat tail extending beyond the limit of the figure, so that even 100 angular division points will not be sufficient to evaluate the integral exactly. The profiles 5 and 6 give the expansion coefficients of the phase function truncated at $\Theta_t=10°$ and 15°, respectively, by using Eq. (5). Now these expansion do not have the extending tail. Especially for profile 6, about 30 angular division points will be sufficient.

It is worth noting that the coefficient α_1 divided by three gives the asymmetry factor of phase function, that is,

$$\langle \cos\Theta \rangle = \frac{1}{2}\int_{-1}^{1} P(\cos\Theta)\cos\Theta d(\cos\Theta) = \frac{1}{3}\alpha_1 . \qquad (7)$$

The asymmetry factors for the phase functions denoted by profiles 1, 2, 3, 4, 5 and 6 in Fig. 3 are 0.84534, 0.76752, 0.72898; 0.95425, 0.93939 and 0.92312, respectively. The truncation approximation naturally reduces the asymmetry of the phase function.

3. Computational scheme

Calculation of the radiative transfer in a homogeneous plane parallel layer has been carried out by using the matrix method (Plass et al., 1973). Transmitted and reflected fluxes from the layers with different optical thicknesses and single scattering albedos were computed for various incidence of a parallel beam of radiation.

Commonly used method of renormalization of the phase matrix (Wisombe, 1976)

for flux conservation in the doubling method will turn out to be unsuitable for a large set of the angular division points. So we propose a new method of renormalization using an iterative procedure. Computed values of the phase matrix $P_{ij}{}^{+\pm} \equiv \int_0^{2\pi} P(\pm\mu_i\mu_j + \sqrt{1-\mu_i^2}\sqrt{1-\mu_j^2}\cos\varphi)d\varphi$ are used as initial values of iteration. Here $\mu = \cos\theta$, θ and φ are the zenith and azimuth angles, respectively, and i and j are from 1 to N; N is the total number of the discrete division points for angular integration over the interval [0, 1]. The superscirbed signs + and − represent the upward ($+\mu_j$) and downward ($-\mu_j$) directions, respectively. Then, iterative calculations are repeated, until some convergence criterion is achieved, as follows,

$$
\begin{aligned}
&P_{ij}{}^{(1)+\pm} = P_{ij}{}^{+\pm}\,, \\
&S_i{}^{(n)} = \sum_{j=1}^{N} (P_{ij}{}^{(n)++} + P_{ij}{}^{(n)+-})c_j\,, \\
&P_{ij}{}^{(n+1)+\pm} = \frac{1}{2}\left(\frac{1}{S_i{}^{(n)}} + \frac{1}{S_j{}^{(n)}}\right) P_{ij}{}^{(n)+\pm}\,,
\end{aligned}
\tag{8}
$$

where C_j's are the weight coefficients of quadrature and the superscript (n) indicates the iteration steps. It is easily proved that, by this procedure, the phase matrix $P_{ij}{}^{+\pm}$ converges to a limit value conserving the symmetric property of the phase matrix $P(\mu_i, \mu_j) = P(\mu_j, \mu_i)$.

Because the number of the angular division points N must be very large in calculations with the untruncated complete phase function, we must check convergence of the computed flux values with respect to N. In the calculation, the interval $\mu\in[0, 1]$ were divided into five subintervals with equal spacing of $\Delta\mu=0.2$. Then the shifted Gaussian quadrature of an odd order was applied to each subinterval so as to evaluate the fluxes at common incident angular points $\mu_0=0.1$, 0.3, 0.5, 0.7, and 0.9, which are values of the center of five subintervals. With this quadrature scheme, we have calculated a series of flxues for five values of N as 35, 45, 65, 75, and 85.

Fig. 4 shows the relative difference in percent between fluxes calculated with different values of N and with $N=85$, as a function of N, i.e.,

$$
\varepsilon F_N{\uparrow\downarrow} = F{\uparrow\downarrow}(\tau, N)/F{\uparrow\downarrow}(\tau, N=85) - 1\,, \tag{9}
$$

where τ is the optical thickness of the layer and the upward and downward arrows indicate the reflected and transmitted fluxes, respectively. By difinition, $\varepsilon F{\uparrow\downarrow}=0$ for $N=85$. Value of the optical thickness τ, hereafter, refers to the layer with the untruncated complete phase function. This figure displays the integration accuracy for the transmitted fluxes (by solid lines) and reflected ones (broken lines) from the conservative layer having the complete hydrosol phase function shown in Fig. 2 and with the optical thickness $\tau=32$, for several incident angles μ_0. The integration error for both transmitted and reflected fluxes increases as the incident direction approaches the zenith. The transmitted fluxes computed with smaller N are larger,

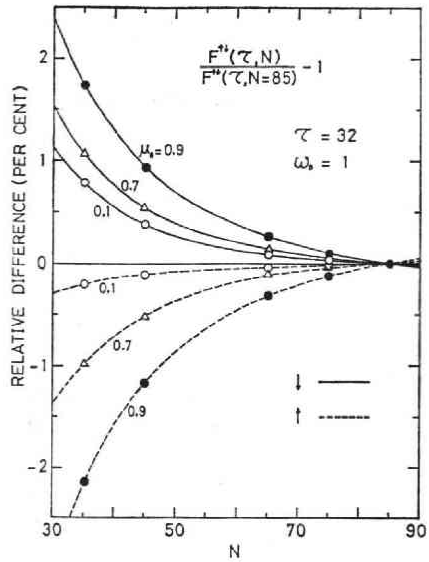

Fig. 4. Relative differences between the fluxes calculated with different number of angular division points N and with $N=85$, as a function of N. The solid and broken lines indicate results, respectively, for the transmitted and reflected fluxes from the conservative layer of the optical thickness $\tau=32$ having the complete hydrosol phase function for several values of cosine of the incident angle μ_0.

on the other hand, the reflected ones are smaller. With an increase of N, as expected, the magnitude of the relative difference $\varepsilon F^{\uparrow\downarrow}$ monotonously decreases; the flux approaches an asymptotic value or a true value for $N\to\infty$. We have estimated the true values of the emerging fluxes from the layers with the complete phase functions for cloud and hydrosols by an extrapolation method; the detailed procedure is not shown here for simplicity. Error involved in the estimated *true* flux values is probably less than 0.5%. Fluxes computed with $N=85$ differs 5%, at the most, from the estimated *true* ones $F^{\uparrow\downarrow}(\tau, N=\infty)$. The difference is larger for larger μ_0 and smaller w_0. Fig. 5 shows the relative difference of the emerging fluxes computed with $N=45$ from the estimated *true* fluxes as a function of the optical thickness of the layer. This figure is for the transmitted (solid lines) and reflected (broken lines) fluxes from the conservative ($w_0=1$, upper curves) and absorbing ($w_0=0.5$, lower curves) layers having the complete hydrosol phase function for different incident angles of $\mu_0=0.1$, 0.7 and 0.9. The integration error for transmission increases as the optical thickness increases, and as the absorptivity of the layer increases. Error for reflection from the conservative layer decreases with increase of the optical thickness but for the absrobing layer it becomes independent of the optical thickness. Both for transmission and reflection, the integration error is larger for larger μ_0. This feature is already shown in Fig. 4 and may be attributed to the fact that when the incident angle μ' approaches to the zenith or $\mu'\to 1$, numerical quadrature of the angular integration in the matrix method becomes more difficult because the phase function $P(\mu\mu'+\sqrt{1-\mu^2}\sqrt{1-\mu'^2}\cos\varphi)$ becomes

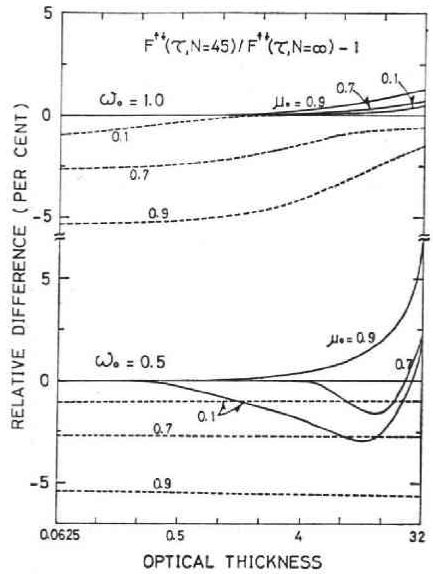

Fig. 5. Relative differences between the fluxes calculated with $N=45$ and the estimated true fluxes ($N=\infty$), as a function of optical thickness, for the conservative ($w_0=1$) and absorptive ($w_0=0.5$) hydrosol layers. The solid and broken lines indicate results for the transmitted and reflected fluxes, respectively.

more rapidly varing function with μ.

Behavior of the integration error for cloud layers are similar to that for hydrosol layers. For the truncated phase function, the quadrature with the angular division points $N=85$ is accurate enough.

4. Results and Discussions

With the computational scheme mentioned above, we have estimated the relative error introduced in the fluxes by the truncation approximation,

$$\varepsilon F^{\uparrow\downarrow} = F_t^{\uparrow\downarrow}/F_0^{\uparrow\downarrow} - 1 \,, \tag{10}$$

where F_0 and F_t are the emerging fluxes computed with the complete and truncated phase functions, respectively. The upward and downward arrows indicate, respectively, the reflected and transmitted fluxes from the layer.

Fig. 6 shows the relative error $\varepsilon F^{\uparrow\downarrow}$ for the layers with the hydrosol phase function truncated at $\theta_t=15°$, as a function of the optical thickness τ, for several values of the incident direction μ_0 and the single scattering albedo w_0. Errors for transmission are pictured by solid lines and those for reflection by borken lines. Corresponding figure for the layers with the truncated cloud phase function at $\theta_t=15°$ is shown in Fig. 7. Values of the single scattering albedo were set to be 1.0, 0.5 and 0.1 for the hydrosol layers and 1.0 and 0.5 for the cloud layers. Since errors for reflection with $w_0=0.1$ are almost independent of τ, we have omitted them in Fig. 6.

From these figures, first of all, we can see that almost all errors due to the

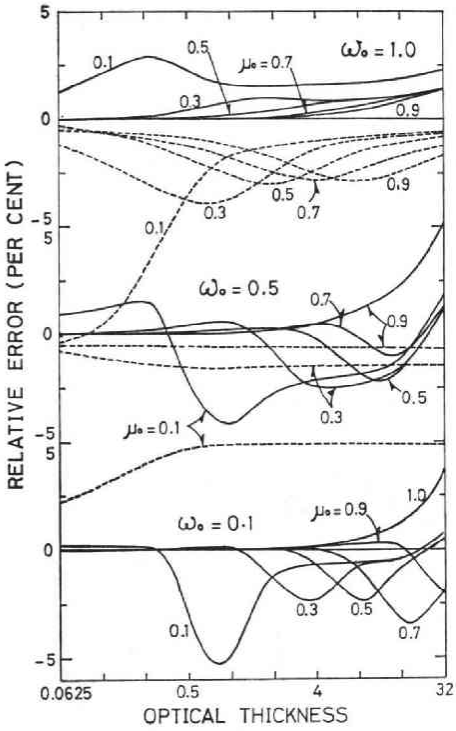

Fig. 6

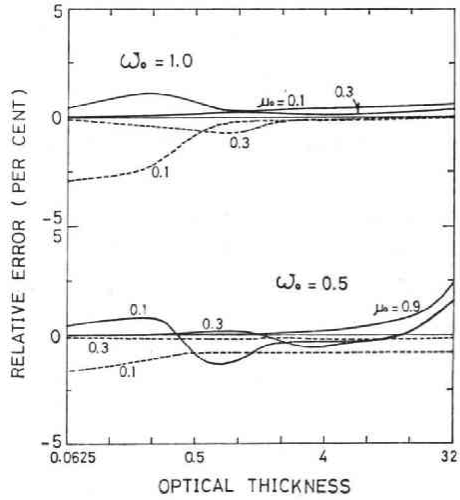

Fig. 7

Fig. 6. Relative errors introduced by the peak truncation approximation in the transmitted (solid lines) and reflected (broken lines) fluxes from the hydrosol layers as a function of the optical thickness for the complete hydrosol phase function. The truncated phase function is that for hydrosols with $\theta_t = 15°$ (curve 6 in Fig. 2). Results are shown for the conservative ($w_0 = 1$) and absorptive ($w_0 = 0.5$ and $w_0 = 0.1$ (only for transmission)) layers, and for several values of μ_0. The ordinate is on a logarithmic scale.

Fig. 7. Same as Fig. 6, but for the truncated cloud phase function at $\theta_t = 15°$ (curve 3 in Fig. 1). For simplicity, curves for $\mu_0 = 0.9$, 0.3 and 0.1 are only shown for the cloud layers of $w_0 = 1$ and 0.5. See legend to Fig. 6.

truncation approximation for both reflection and transmission are smaller than 5% for the hydrosol layers and than 1.5% for the cloud layers. Same analysis reveals that errors $\varepsilon F\uparrow\downarrow$ for the hydrosol phase function truncated at $\theta_t = 10°$ are much smaller and less than 1.5% and that those for the cloud phase function truncated at $\theta_t = 6°$ are less than 0.5%. Truncation approximation introduces less errors for the cloud-type phase function than for the hydrosol-type phase function: radiative transfer in the cloud layer is less affected by the truncation of the forward peak of phase function than in the hydrosol layer.

Secondly, it is interesting to know that error profiles change very complicatedly but systematically with τ, μ_0 and w_0. Such a behavior is not a random one, which we frequently encounter in the analysis of calculation error, but it is caused by a physical effect of the truncation of the phase function, so that an interpretation of the behavior of error profile by an elementary concepts of the radiative transfer will help us to

understand the mechanism of radiative transfer in the cloud and hydrosol layers. Hence, hereafter, we will investigate the behavior of the error profile in detail.

Following the parameter key of μ_0, we know that for both reflection and transmission the profile systematically shifts toward larger τ as the direction of incidence approaches the zenith. This is because the effective optical thickness of the layer becomes smaller for a radiation propagating along less slant path, so that the thickness of the layer bringing the same phenomenon must be larger for such a radiation. The profile for reflection with $w_0=1$ approaches the zero line when τ is sufficiently small or large, and it has an extremum at a medium value of τ, with an exception of the profile for $\mu_0=0.1$, which does not approach the zero line as τ becomes small. To understand these behaviors of the profile, we consider a schematic diagram for three characteristic directions of incidence as shown in Fig. 8, where the truncated part of phase function is schematically shaded. If the layer is sufficiently thin and the direction of incidence is not too slant, the scattering as shown in case (II) predominantes and the reflected radiation mainly consists of the backwardly scattered radiation by the untruncated part of the phase function, so that the error introduced in the reflected fluxes by the truncation is small. Even for such a thin layer, if the direction of incidence is very slant, the scattering in case (I) predominates and the considerable portion of the reflected flux should be attributed to the single scattered radiation from the truncated part of the phase function. The truncation procedure injects this portion as an unscattered radiation into the layer, so that the error does not reduce to zero even for a sufficiently thin layer. As the thickness of the layer

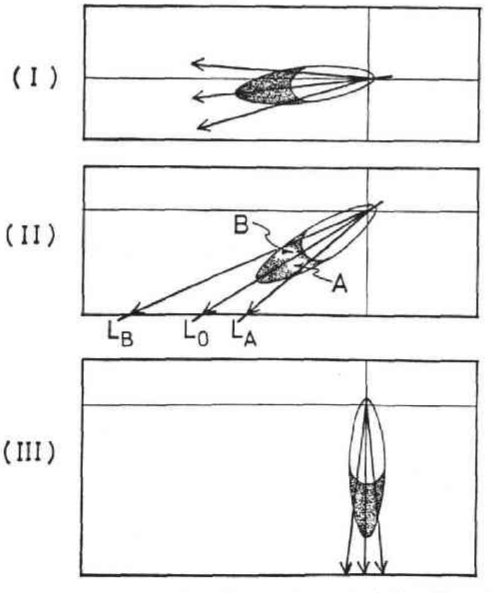

Fig. 8. Schematic scattering diagrams for three characteristic directions of incidence. The shaded area indicates schematically the truncated forward peak of phase function, which consists of two parts A and B propagating along the lower and upper paths L_A and L_B, respectively.

increases, part of the forward-scattered radiation will reappear from the upper surface through the multiple scattering. Radiation injected deeper into the layer by the truncation may transmit the layer before it becomes the reflected radiation. Hence the truncation approximation underestimates the reflected flux and the error $\varepsilon F\uparrow$ becomes a negative large value, i.e. the reflectivity of the layer decreases by the truncation. As the thickness of the layer increases further and becomes sufficiently large, the injected radiation will be also reflected through the multiple scattering process, and then the error is diminished.

Next, we shall look at errors $\varepsilon F\uparrow$ for transmission in Figs. 6 and 7. The behavior of $\varepsilon F\downarrow$ for $w_0=1$ can be interpreted in contrast with that for reflection because the flux conservation is well established in the truncated system. If absolute errors for transmission and reflection were pictured their profiles would be entirely symmetrical. The profiles for the absorbing layers with $w_0=0.5$ and 0.1, however, need some other interpretation. Common characteristics for these profiles are following: the error reduces to zero for a sufficiently thin layer, it increases to a positive value as the thickness of the layer increases, and then it decreases to a negative value at a medium thickness, and again it increases infinitely as the thickness further increases. This characteristic behavior is more evident for the layers with lower w_0. A simple interpretation of this behavior is proposed with the help of the illustration in Fig. 8. For a thin layer in which the single scattering is prevailing, both of the radiations in parts A and B propagating along the paths L_A and L_B respectively, can contribute to the transmitted flux. Since these radiations are assumed to be unscattered and to propagate along the same path L_0 in the truncation approximation, the contribution of radiation in part A to the transmitted flux may be underestimated and the contribution of B may be overestimated. Difference of the path length between L_B and L_0 is larger than that between L_0 and L_A, so that the overestimation effect of B surpasses the underestimation effect of A. Hence, the transmitted flux is overestimated by the truncation, $\varepsilon F\downarrow$ becomes a positive value. For an intermediately thick layer, radiation in part B along the longer path L_B becomes negligible. Then, the underestimation of A predominates, and therefore the transmitted flux is weakened by the truncation, i.e. $\varepsilon F\downarrow$ becomes a negative value. Finally for sufficiently thick layer, the radiation propagating in vertical direction as shown in (III) predominantes deep in the layer (Kattawar and Plass, 1976). Since the truncation procedure injects the scattered radiation deeper into the layer, the transmitted flux is intensified by the truncation, i.e., $\varepsilon F\downarrow$ becomes a positive value. In the case of vertical incidence, scattering in case (III) of Fig. 8 always predominantes and the error profile becomes a monotonous increasing function of τ as shown, for exmaple, for $\mu_0=0.9$ with $w_0=0.5$ and for $\mu_0=1$ with $w_0=0.1$.

From the figures the relative error $\varepsilon F\downarrow$ for transmission seems to be increasing for much larger τ, however, the absolute error in the transmitted flux will be unimportant because the transmitted flux itself becomes very small for such large optical thicknesses.

Figs. 9 and 10 shows errors $\varepsilon F\uparrow\downarrow$ for the truncation at $\theta_t=15°$, as a function of μ_0,

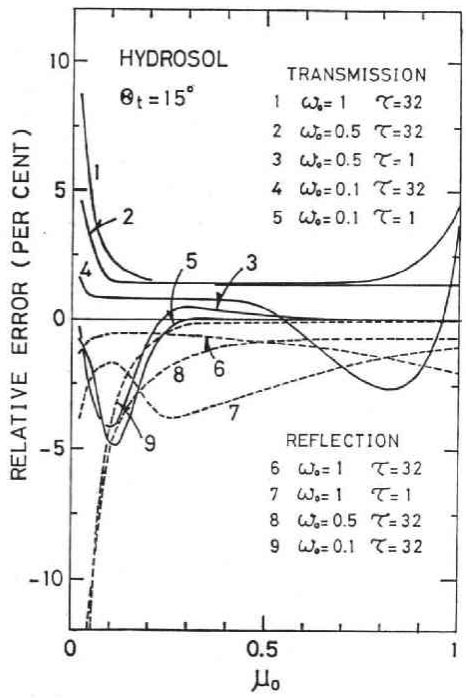

Fig. 9

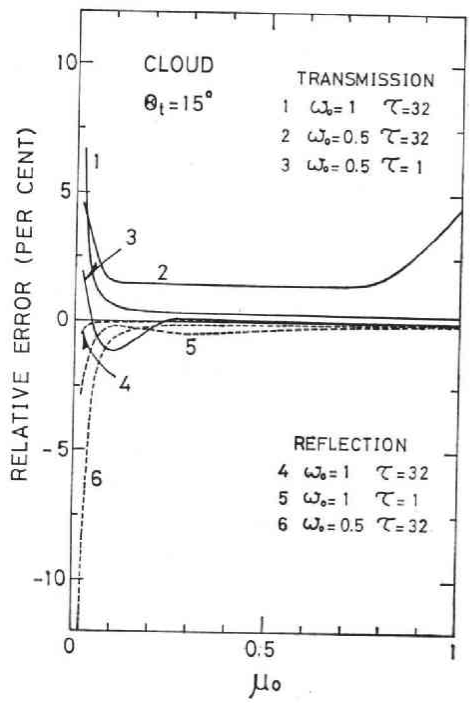

Fig. 10

Fig. 9. Relative errors due to the peak truncation approximation for the hydrosol layer as a function of cosine of the incident zenith angle μ_0. The truncated phase function is that for hydrosols with $\theta_t = 15°$. Solid lines indicate errors for transmission and broken lines ones for reflection.

Fig. 10. Same as Fig. 9, but for the truncated cloud phase function at $\theta_t = 15°$.

for the hydrosol and cloud layers, respectively. The error for transmission $\varepsilon F\downarrow$ is given by solid lines and that for reflection $\varepsilon F\downarrow$ by broken lines. Comparison between these two figures reveals that main feature of error profiles with respect to μ_0 is in farily well agreement, although the absolute values of error for the hydrosol layer are much larger than those for the cloud layer. For optically thick conservative layers with $\tau = 32$, error $\varepsilon F\downarrow$ for transmission is generally positive, while $\varepsilon F\uparrow$ for reflection is negative. For thick absorbing layer ($\tau = 32$, $w_0 = 0.5$), error profile for transmission has a broad minimum in the region $0.1 \lesssim \mu_0 \lesssim 0.7$, and it grows as $\mu_0 \to 1$, whereas that for reflection approaches a small limiting value. For thin absorbing layer ($\tau = 1$, $w_0 = 0.5$ and $w_0 = 0.1$), $\varepsilon F\downarrow$ takes negative values around $\mu_0 = 0.1$. In the region of $\mu_0 = 0.1$, absolute values of both $\varepsilon F\downarrow$ and $\varepsilon F\uparrow$ rapidly increase, as $\mu_0 \to 0$, without respect to w_0 and τ. Rapid increase of $\varepsilon F\downarrow$ and $\varepsilon F\uparrow$ as $\mu_0 \to 0$ has been already discussed by Hansen and Potter, but the increase of $\varepsilon F\downarrow$ for absorbing thick layer as $\mu_0 \to 1$ has not been noted yet.

These behaviors of error profiles with respect to μ_0 can be understood from the previously proposed interpretations for Figs. 6 and 7, supposing that $1/\mu_0$ may play a same role as the optical thickness of the layer and that the truncation approximation may inject a scattered radiation by the shaded part of the phase function shown in

Fig. 8 into the layer as an unscattered radiation. Of course, it should be noticed that radiative transfer in the layer is not a single scattering process, but a multiple scattering process: this makes the behavior of error profile complicated and dimmed.

5. Summary

We have estimated the relative errors of the emerging fluxes from the cloud and hydrosol layers by solving the multiple scattering problem for a characteristic phase function with and without a sharp forward peak. And we have proposed a physical interpretation for the error profiles by considering a simple scattering model.

Errors in the emerging fluxes from the cloud layer are smaller than those for the hydrosol layer; because considerable portion of the truncated part of the cloud phase function concentrates around a smaller scattering angle than that for the hydrosol phase function. For the same layer, of course, the approximation brings a larger error for the peak truncation at a larger scattering angle Θ_t or for a larger truncation ratio S_t. For almost all parameter values used here, the relative errors in fluxes seldom exceed, respectively, 1.5% and 0.5% for the cloud phase functions truncated at $\Theta_t=15°$ and 6°, and those for the hydrosol phase functions truncated at $\Theta_t=15°$ and 10° are within 5% and 1.5%, respectively.

Behaviors of error profiles for the reflected and transmitted fluxes are complicated but systematic. For conservative layer ($w_0=1$), the flux transmissivity is a little intensified by the truncation approximation, while the reflectivity is diminished. For a absorbing layer, the relative errors $\varepsilon F\uparrow$ for the reflected flux are still negative and are almost indpendent of the optical thickness, while errors $\varepsilon F\downarrow$ for the transmitted flux become negative for a medium optical thickness depending on an incident angle μ_0. A significant error both in the reflection and transmission occurs for a very slant incidence as $\mu_0 \lesssim 0.1$, without respect to τ and w_0.

In general, errors introduced by the peak truncation approximation in fluxes are small enough for widely varying values of the incident angle, optical thickness and absorption, and they will be unimportant for most applications. This assures the usefulness of the peak truncation approximation in the multiple scattering problem with a phase function having a sharp forward peak.

References

Chandrasekhar, S., 1960: Radiative Transfer, Dover Publication, Inc., New York.

Hansen, J.E. 1969: Exact and approximate solutions for multiple scattering by cloudy and hazy planetary atmosphere, *J. Atmos. Sci.*, **26**, 478–487.

Kattawar, G.W. and G.N. Plass, 1976: Asymptotic radiance and polarization in optically thick media: ocean and clouds, *Appl. Opt.*, **15**, 3166–3178.

Plass, G.N., G.W. Kattawar and F.E. Catchings, 1973: Matrix operator theory of radiative transfer I, *Appl. Opt.*, **12**, 314–329.

Potter, J.F. 1970: The delta function approximation in radiative transfer theory, *J. Atmos. Sci.*, **27**, 943–949.

Tanaka, M., S. Asano and G. Yamamoto, 1976: Transfer of solar radiation through water clouds, *Proc. International Radiation Symposium*, Garmisch-Partenkirchen, Aug. 18–30, 1976.

Tanaka, M. and T. Nakajima, 1977: Effects of oceanic turbidity and index of refraction of hydrosols on the flux of solar radiation in the atmosphere-ocean system, *J. Quant. Spectrosc. Radiat. Transfer*, **18**, 93–111.

Wiscombe, W.J., 1976: On initialization, error and flux conservation in the doubling method, *J. Quant. Spectrosc. Radiat. Transfer*, **16**, 637–658.